Modifying L-Type Calcium Current Kinetics: Consequences for Cardiac Excitation and Arrhythmia Dynamics

Aman Mahajan,*† Daisuke Sato,* Yohannes Shiferaw,‡ Ali Baher,* Lai-Hua Xie,* Robert Peralta,* Riccardo Olcese,*† Alan Garfinkel,* Zhilin Qu,* and James N. Weiss*

*UCLA Cardiovascular Research Laboratory and the Division of Molecular Medicine, †Departments of Anesthesiology, Medicine (Cardiology), Physiology and Physiological Science, David Geffen School of Medicine at UCLA, Los Angeles, California; and ‡Department of Physics and Astronomy, California State University, Northridge, California

ABSTRACT The L-type Ca current ($I_{Ca,L}$), essential for normal cardiac function, also regulates dynamic action potential (AP) properties that promote ventricular fibrillation. Blocking $I_{Ca,L}$ can prevent ventricular fibrillation, but only at levels suppressing contractility. We speculated that, instead of blocking $I_{Ca,L}$, modifying its shape by altering kinetic features could produce equivalent anti-fibrillatory effects without depressing contractility. To test this concept experimentally, we overexpressed a mutant Ca-insensitive calmodulin (CaM_{1234}) in rabbit ventricular myocytes to inhibit Ca-dependent $I_{Ca,L}$ inactivation, combined with the ATP-sensitive K current agonist pinacidil or $I_{Ca,L}$ blocker verapamil to maintain AP duration (APD) near control levels. Cell shortening was enhanced in pinacidil-treated myocytes, but depressed in verapamil-treated myocytes. Both combinations flattened APD restitution slope and prevented APD alternans, similar to $I_{Ca,L}$ blockade. To predict the arrhythmogenic consequences, we simulated the cellular effects using a new AP model, which reproduced flattening of APD restitution slope and prevention of APD/Ca_i transient alternans but maintained a normal Ca_i transient. In simulated two-dimensional cardiac tissue, these changes prevented the arrhythmogenic spatially discordant APD/Ca_i transient alternans and spiral wave breakup. These findings provide a proof-of-concept test that $I_{Ca,L}$ can be targeted to increase dynamic wave stability without depressing contractility, which may have promise as an antifibrillatory strategy.

INTRODUCTION

The L-type Ca current ($I_{Ca,L}$) regulates excitation-contraction coupling and action potential (AP) repolarization, both essential functions for contraction and relaxation of the heart. The early peak of $I_{Ca,L}$ during the AP controls sarcoplasmic reticulum (SR) Ca release vital for excitation-contraction coupling, whereas the late phase directly influences repolarization. $I_{Ca,L}$ also plays an important role in the development of cardiac arrhythmias such as ventricular fibrillation (VF), the leading cause of sudden cardiac death. Blocking $I_{Ca,L}$ is a potent means of suppressing VF (1,2), but unfortunately the doses of Ca channel blockers required to achieve this effect also severely depress contractility, precluding their clinical usefulness as antifibrillatory drugs. In this study, we used a combined experimental and modeling approach to explore how $I_{Ca,L}$ regulates the complex interactions between excitation-contraction coupling and repolarization, toward the goal of developing a strategy to suppress arrhythmias without impairing excitation-contraction coupling.

Theoretical and experimental studies have identified key mechanisms by which $I_{Ca,L}$ blockade prevents VF, including flattening AP duration (APD) restitution slope, suppressing intracellular Ca (Ca_i) cycling dynamics by unloading SR Ca, and preventing APD and Ca_i alternans (1–4). APD restitution refers to the dependence of APD on the preceding diastolic interval (DI), whereas APD alternans refers to beat-to-beat alternation in APD which increases dispersion of repolarization, especially when it becomes spatially discordant (5–7). Both are strongly influenced by $I_{Ca,L}$ properties, particularly recovery from inactivation (3). During a normal AP, $I_{Ca,L}$ peaks early, triggering robust SR Ca release before partially inactivating due to two processes: Ca-dependent inactivation (CDI), mediated by Ca binding to calmodulin (CaM) tethered to the C-terminus of the channel, and voltage-dependent inactivation (VDI). The rate and degree of inactivation of $I_{Ca,L}$ by these processes during the late phase of the APD has a major influence on repolarization. Current evidence (8,9) suggests that VDI is the fundamental inactivation process, which is inhibited by an interaction of CaM with the C-terminus of the channel's pore-forming α-subunit. When Ca binds to CaM, the conformational change in the Ca-CaM complex relieves this inhibition, causing the channels to inactivate more quickly. After repolarization, L-type Ca channels recover from inactivation with characteristic voltage- and time-dependent kinetics. At fast heart rates, incomplete recovery of $I_{Ca,L}$ before the next beat is an important mechanism shortening APD, which is physiologically essential to preserve diastole for ventricular filling and coronary blood flow. Thus, $I_{Ca,L}$ recovery from inactivation has important effects on the slope of APD restitution, which in turn is a powerful determinant of electrical wave stability. A steep APD restitution slope means that small changes in

Submitted October 2, 2006, and accepted for publication October 3, 2007.

Aman Mahajan, Daisuke Sato, and Yohannes Shiferaw contributed equally to this work.

Address reprint requests to James N. Weiss, MD, Tel.: 310-825-9029; E-mail: jweiss@mednet.ucla.edu.

Editor: David A. Eisner.

0006-3495/08/01/411/13 $2.00

doi: 10.1529/biophysj.106.98590

DI lead to large changes in APD, resulting in APD alternans (repolarization alternans), and thus large alteration in the wavelength (the product of APD and conduction velocity) of the electrical wave, promoting head-tail interactions between successive waves and causing wavebreak initiating spiral wave reentry (5,6).

Ca_i cycling dynamics also has important effects on APD mediated through Ca_i-sensitive currents including both $I_{Ca,L}$ inactivation by CDI and electrogenic Na-Ca exchange (10). Hence, Ca_i cycling dynamics producing beat-to-beat variations in the Ca_i transient amplitude can also induce repolarization gradients leading to wavebreak. The effect of $I_{Ca,L}$ inactivation kinetics on Ca_i cycling dynamics process has not been explored in detail, but is likely to be important since Ca entry via $I_{Ca,L}$ is a major determinant of SR Ca loading, which strongly influences Ca_i cycling dynamics (10).

When $I_{Ca.L}$ is blocked, both simulation and experimental studies (1–4) have demonstrated that APD restitution slope becomes flatter, APD alternans is suppressed, and spiral wave breakup is prevented. However, the theoretical studies suggest that it is the kinetics of $I_{Ca,L}$ recovery, rather than its amplitude per se, that modulates its effects on APD restitution slope (6). This raises the possibility that instead of blocking $I_{Ca,L}$, modifying its shape by altering its inactivation kinetics might produce equivalent effects on dynamic wave stability without depressing the Ca_i transient and contractility. Because modifying $I_{Ca,L}$ inactivation kinetics produces complicated effects on both AP properties and excitation-contraction coupling, we adopted a combined experimental and mathematical modeling approach. To develop the experimental strategy, we suppressed $I_{Ca,L}$ inactivation by overexpressing a Ca-insensitive calmodulin mutant (CaM_{1234}) to inhibit CDI in rabbit ventricular myocytes (11). Since CaM_{1234} overexpression also significantly prolongs APD (11), we shortened APD back to control levels using either the ATP-sensitive K current (I_{KATP}) agonist pinacidil, or the $I_{Ca,L}$ blocker verapamil. Both interventions flattened APD restitution slope and prevented APD alternans. Furthermore, the combination of CaM_{1234} overexpression with pinacidil enhanced cell shortening, whereas as the combination with verapamil suppressed cell shortening. To investigate the underlying mechanisms of these cellular effects, we employed a new rabbit ventricular AP model (12), based on Shannon et al. (13), with two important modifications: 1), incorporation of a new Markovian formulation of $I_{Ca,L}$, based on physiological experimental data from rabbit ventricular myocytes, which explicitly separates the CDI and VDI components of inactivation; and 2), replacement of the Ca_i cycling machinery (which has trivial dynamics in the existing model) with the dynamic Ca_i cycling model described by Shiferaw et al. (14). This AP model was tuned to reproduce APD restitution characteristics and APD and Ca_i alternans in rabbit ventricle, as described in a previous article (12). Using this AP model, we found that inhibiting CDI prolonged APD. If APD was then returned to normal by activating I_{KATP} and partially blocking $I_{Ca,L}$, the combined intervention maintained a normal Ca_i transient amplitude, but flattened APD restitution slope, suppressed Ca_i cycling alternans and prevented APD alternans, similar to the experimental results in myocytes. Moreover, in two-dimensional tissue simulations, these cellular effects suppressed the development of spatially discordant alternans, a highly arrhythmogenic substrate which can initiate spiral wave reentry (5,6,10), and also prevented spiral wave breakup.

This study provides insight into how the shape of $I_{Ca,L}$ dually influences excitation-contraction coupling and repolarization of the cardiac AP, and suggests, at the proof-of-concept level, that modification of $I_{Ca,L}$ may be promising as an anti-VF strategy.

METHODS

All animal procedures conformed to the ''Guiding Principles for Research Involving Animals and Human Beings'' of the American Physiological Society.

Preparation of left ventricular myocytes

Rabbit cardiac myocytes were isolated as described previously (15). Briefly, hearts were rapidly excised from 2 to 3 kg New Zealand white rabbits anesthetized with intravenous pentobarbital, and submerged in Ca-free Tyrode's solution containing (in mmol/L) 140 NaCl, 5.4 KCl, 1 $MgCl_2$, 0.33 NaH_2PO_4, 10 glucose, and 5 HEPES adjusted to pH 7.4. The aorta was cannulated and the heart perfused retrogradely at 37°C on a Langendorff apparatus with Ca-free Tyrode's buffer containing 1.65 mg/mL collagenase (Sigma Blend H C-8051; Sigma, St. Louis, MO) and 0.8 mg/mL bovine albumin (Sigma A-8806) for 30–40 min. All solutions were continuously bubbled with 95% O_2–5% CO_2. After washing out the enzyme solution, the hearts were removed from the perfusion apparatus, and swirled in a beaker. The Ca concentration was slowly increased to 1.8 mmol/L, and the cells were stored at room temperature. This procedure typically yielded 50% rod-shaped Ca-tolerant myocytes. For acute use, Ca-tolerant, rod-shaped ventricular myocytes with clear striations were randomly selected for electrophysiological studies within 8 h of isolation.

Cellular electrophysiological studies

Macroscopic voltage and currents were recorded under the current and voltage-clamp conditions using the whole cell perforated patch configuration. Perforated patches were formed using the amphotericin method (16), in which the patch pipette was dipped for 10 s into the pipette solution. The pipette was then back-filled using the same solution containing 240 μg/mL amphotericin-B (Sigma, cat. no. A4888). Electrodes (Garner Glass, Claremont, CA) had a tip diameter of 2–3 μm and resistance of 1–4 MΩ. A DigiData 1200 (Axon Instruments, Foster, CA) controlled by pCLAMP software (Axon Instruments) was used to generate command pulses and acquire data.

For current-clamp action potential recordings, the pipette solution contained (in mmol/L): 140 K-Aspartate, 5 NaCl, 10 HEPES, 1 EGTA, 5 MgATP, 5 creatine phosphate, and 0.05 cAMP; pH 7.2 with HCl. The bath contained standard Tyrode's solution with 140 NaCl, 5.4 KCl, 1.8 $CaCl_2$, 1 $MgCl_2$, 0.33 NaH_2PO_4, 10 glucose, and 5 HEPES adjusted to pH 7.4. For voltage-clamp experiments measuring $I_{Ca,L}$, K-aspartate was replaced with CsOH in the pipette solution, and rabbit ventricular myocytes were

superfused with a HEPES-buffered Tyrode solution containing (in mmol/L) 135 NaCl, 5.4 KCl, 1 MgCl, 2 $CaCl_2$, 5 HEPES, and 10 glucose, with pH adjusted to 7.3 with NaOH. In some experiments, $CaCl_2$ was replaced with 1.8 mM $BaCl_2$, and uptake and release of Ca from the sarcoplasmic reticulum (SR) were suppressed by preincubating the myocytes for 30–60 min with 10 μmol/L ryanodine and 2 μmol/L thapsigargin. All electrophysiology experiments were performed at physiologic temperatures (35–37°C).

Voltage-clamp protocols for measuring $I_{Ca,L}$

Activation and inactivation kinetics of $I_{Ca,L}$ were recorded using a square pulse protocol that delivered test step pulses from −40 to +50 mV in 10 mV increments from a holding potential of −80 mV. Na currents were inactivated by a prepulse step (−80 mV to −40 mV, 40 ms) and by the inclusion of 10 μmol/L tetrodotoxin in the superfusate.

APD restitution protocol

To measure dynamic APD restitution, the myocyte was paced at a cycle length (CL) of 400 ms until steady-state APD was reached, after which the CL was progressively decreased by 5–20 ms after every 12 beats, until 2:1 block occurred. For cells transfected with Ad-CaM_{1234} that had markedly prolonged APD, initial pacing CL was 3–5 s. APD was measured at 90% repolarization (APD_{90}), and the DI was calculated as CL minus APD_{90}. For both dynamic and S1S2 methods, APD restitution curves were constructed by plotting APD_{90} versus DI, and the data points were best fit to a single exponential. The maximum APD restitution slope was calculated from the first derivative of the fitted exponential curve at the shortest DI which captured.

Gene transfer

Expression vector

cDNAs for the human and/or rabbit cardiac α_{1C} and β-subunits of the L-type Ca channel were subcloned into the vector pCDNA3amp (Invitrogen, Carlsbad, CA). To demonstrate expression in HEK293 cells, these constructs were cotransfected with GFP (pEGFP vector from Clontech, Palo Alto, CA) at ratios of ~1:10. Both vectors used the CMV promoter. Replication-deficient recombinant adenoviral constructs containing wild-type CaM (Ad-CaM_{wt}) and Ca-insensitive mutant CaM_{1234} (Ad-CaM_{1234}) also expressing GFP through an internal ribosome entry site motif (11) were kindly provided by Dr. David Yue's laboratory. The recombinant viruses were amplified using HEK293 cells, with five cycles of amplification harvesting, using a freeze-and-thawing method and final purification with CsCl to achieve a final viral particle concentration of ($10^{10–11}$) particle forming units (pfu).

Gene expression in isolated ventricular myocytes

Isolated adult rabbit ventricular were superfused with 1.8 mmol/L Ca Tyrode's solution and prepared for transfection with the Ad-CaM_{1234} adenoviral construct. Myocytes in suspension were centrifuged for 3 min at 250 rpm and 25°C and washed in Dulbecco's modified eagle medium with 10% fetal bovine serum and 1% penicillin/streptomycin until the majority of cellular debris had been removed. Two milliliter aliquots (average density of 100,000–200,000 cells/ml) were plated and incubated in 5% CO_2 at 37°C. After substituting serum-free Dulbecco's modified eagle medium, the Ad-CaM_{1234} construct (~10^9–10^{10} particles/ml) was added to achieve a multiplicity of transfectivity of 10 and, after overnight incubation, replaced with fresh serum-free media. Robust transgene expression with transfection rates of ~85–95%, as monitored by GFP fluorescence, were regularly observed after 36–48 h.

Simulations and numerical methods

We used a physiologically based ionic model described recently (12), modified to include two additional low-affinity Ca buffers (ATP and SL), as described in Shannon et al. (13). The rabbit model is based on ionic currents due to Shannon et al. (13), and incorporates a new Markovian formulation of $I_{Ca,L}$ based on our own experimental data, which explicitly separates Ca- and voltage-dependent components of inactivation. Ca_i cycling is described using the model of Shiferaw et al. (14). This AP model was tuned to reproduce the APD restitution characteristics, APD alternans, and Ca_i dynamics of rabbit ventricular myocytes (12).

Modeling inhibition of Ca-induced inactivation with CaM_{1234}

The L-type Ca current was modeled using a seven-state Markov model described previously (12), which explicitly formulates VDI and CDI consistent with recently proposed molecular mechanisms (8,9). We modeled the effect of CaM_{1234} overexpression by assuming that the overexpressed CaM_{1234} displaced the wild-type CaM in a fraction α of L-type Ca channels in the cell, such that this population of channels exhibited VDI but not CDI. Thus, we let the total Ca current in the cell to have two components: 1), Ca channels which are not affected by the adenovirus and which exhibited the same kinetics as native channels (CDI intact); and 2), Ca channels in which CDI is turned off, such that inactivation occurs more slowly by VDI, with kinetics similar to those with Ba in place of Ca as the charge carrier. Hence, we model the modified total L-type Ca current as

$$I_{Ca}^{CaM} = (1-\alpha)I_{Ca+CDI} + \alpha I_{Ca-CDI}, \tag{1}$$

where I_{Ca+CDI} denotes the current due to native channels with CDI intact, and $I_{Ca\text{-}CDI}$ denotes the contribution of the fraction α of channels which exhibit only VDI. The effect of this change is to substantially enhance the baseline Ca current, since a larger fraction of channels do not inactivate rapidly via CDI.

Modeling the effect of pinacidil

To model the effects of pinacidil, we incorporated the ATP-sensitive K current (I_{KATP}), which is known to be activated by pinacidil (17). This current is modeled, following Shaw and Rudy (18), using

$$I_{KATP} = g_{katp} \cdot \left(\frac{[K^+]_o}{[K^+]_{o,n}}\right)^{0.24} \left(\frac{1}{1+(A_{atp}/K_{atp})^2}\right)(V-E_K), \tag{2}$$

where $g_{katp} = 0.663$ mS/cm^2, $[K^+]_{o,n} = 5.4$ mM, and $A_{atp} = 2$ mM is the intracellular ATP concentration, $K_{atp} = 0.25$ mmol/L is the half-saturation point of the ATP sensitive current, and E_K is the reversal potential for K^+ ions. Under control conditions I_{KATP} is negligible, and the application of pinacidil can be modeled by increasing K_{atp}.

One- and two-dimensional tissue

We modeled a one-dimensional 4.5-cm monodomain cable using the standard cable equation

$$\frac{\partial V}{\partial t} = -\frac{I_{ion}}{C_m} + D\frac{\partial^2 V}{\partial x^2}, \tag{3}$$

and a two-dimensional 7.5 × 7.5 cm^2 monodomain tissue, using the reaction-diffusion equation

$$\frac{\partial V}{\partial t} = -\frac{I_{ion}}{C_m} + D\left(\frac{\partial^2 V}{\partial x^2} + \frac{\partial^2 V}{\partial y^2}\right), \quad (4)$$

where $D = 1.0 \times 10^{-3}$ cm^2/ms is the effective diffusion coefficient of membrane voltage in rabbit cardiac tissue. This yielded a physiologically realistic conduction velocity of 55 cm/s. The reaction-diffusion equation was integrated with an operator splitting method and adaptive time step method (3). The space step was 0.015 cm and the time step varied from 0.1 to 0.01 ms. Spiral waves were initiated using a standard S1S2 cross-field protocol. Spiral tip was defined by the intersection of two iso-voltage lines (at –30 mV) in 1-ms interval and tracked as described previously (19).

Dynamic APD restitution was measured in one-dimensional cables using a similar protocol as in myocytes described above. S1S2 APD restitution curves were also measured in simulated cells only by pacing (S1S1) at a CL of 400 ms until steady state was achieved, and then introducing a premature stimulus (S2) at progressively shorter S1S2 coupling intervals until loss of capture of the S2 stimulus.

Data analysis

The electrophysiological data were analyzed by using Clampfit (Axon Instruments), Excel (Microsoft, Redmond, CA), and Origin (OriginLab, Northampton, MA). Clampfit and Excel were used for the exponential fitting of inactivation and recovery from inactivation kinetics. Other nonlinear curve fittings were performed in Origin. Statistical analysis was performed using *t*-test and ANOVA. *P*-value < 0.5 was considered significant.

RESULTS

Experimental $I_{Ca,L}$ modification by Ad-CaM_{1234} overexpression in isolated rabbit ventricular myocytes

We obtained robust in vitro gene expression in adult rabbit ventricular myocytes in short-term culture when adenoviral constructs ($10^{9–10}$ pfu/mL) expressing GFP were incubated in the culture medium for 36–48 h (Fig. 1 *A*). GFP fluorescence was observed in ~85–95% of myocytes, which retained their rectangular shape and visible striations, whether GFP was expressed alone or linked to either wild-type CaM (CaM_{wt}) or CaM_{1234} in adenoviral constructs.

When GFP-positive myocytes transfected with Ad-CaM_{1234} were voltage-clamped in the perforated patch configuration, peak $I_{Ca,L}$ during a square voltage-clamp pulse to +10 mV averaged 12.0 ± 1.7 pA/pF ($n = 7$), compared to 11.2 ± 1.4 pA/pF ($n = 8$) in nontransfected myocytes. Fig. 1, *B* and *C*, show that $I_{Ca,L}$ inactivated more slowly, with a residual current at the end of a 300 ms voltage-clamp pulse to +10 mV averaging ~40% of the peak value, compared to ~10% for nontransfected myocytes. Inactivation was still biexponential, reflecting both CDI and VDI components, but unlike nontransfected myocytes, the slow VDI component was dominant. The time constant of the slow component (~75 ms) was similar to that obtained when Ba replaced Ca as the charge carrier in nontransfected myocytes treated with ryanodine and thapsigargin to deplete SR Ca (~100 ms).

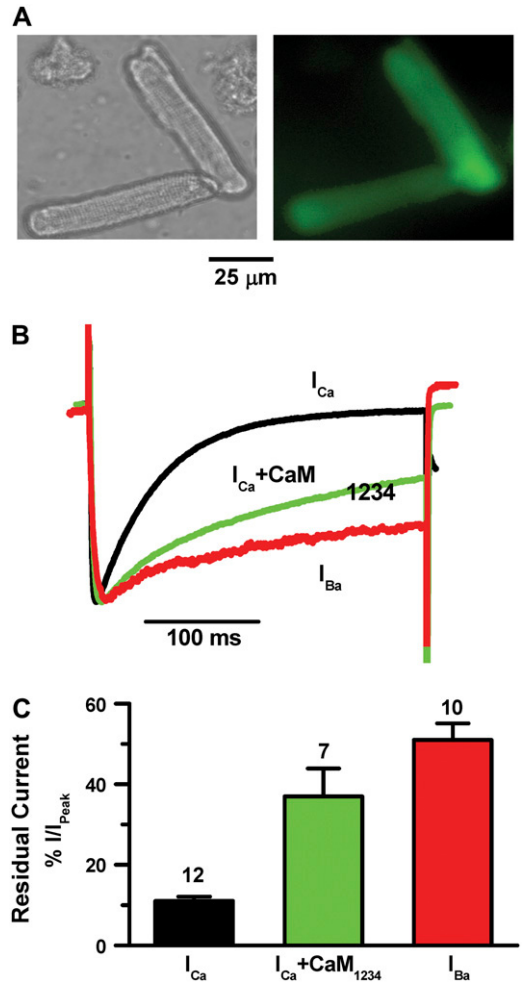

FIGURE 1 (*A*) Adenoviral gene transfer of Ad-CaM_{1234} (containing GFP) into isolated rabbit ventricular myocytes. Upper panels shows bright-field (*left*) and GFP images (*right*) of ventricular myocytes transfected with Ad-CaM_{1234} in vitro after cell isolation. (*B*) Representative normalized traces of I_{Ca} during a 300 ms voltage-clamp pulse from –80 to +10 mV in a nontransfected myocyte (*black*) versus transfected myocyte (*green*), compared to a nontransfected myocyte treated with thapsigargin and ryanodine to deplete SR Ca stores, with external Ba replacing Ca as the charge carrier to eliminate CDI completely (*red*). Data obtained at 37°C using the perforated patch technique. (*C*) Average data summarizing the remaining noninactivated current (relative to peak current) at the end of the 300 ms voltage-clamp, for the number of myocytes indicated above each bar.

These findings are consistent with a fraction of L-type Ca channels bound to CaM_{1234} that exhibit only VDI, and a fraction bound to wild-type CaM which exhibit both CDI and VDI.

To demonstrate that these changes were not an artifact of adenoviral overexpression, we also overexpressed adenoviral constructs containing CaM_{wt} linked to GFP (Ad-CaM_{wt}) or GFP alone (Ad-GFP) in isolated myocytes. Neither constructs caused any significant changes in the CDI or VDI components of $I_{Ca,L}$ inactivation, compared to freshly-isolated nontransfected myocytes (data not shown).

Effects of $I_{Ca,L}$ modification with Ad-CaM$_{1234}$ on APD restitution, APD alternans and cell shortening

Fig. 2 *A* compares representative APs in current-clamped isolated rabbit ventricular myocytes that were either nontransfected, or were transfected with Ad-CaM$_{1234}$ or Ad-CaM$_{WT}$, respectively. APD was significantly prolonged by Ad-CaM$_{1234}$ overexpression, especially at long cycle lengths (CL) (Fig. 2 *B* and Fig. 3 *A*), consistent with previous findings (11). In contrast, APD was not significantly affected by Ad-CaM$_{WT}$ overexpression (Fig. 3 *A*). Fig. 2 *B* shows the rate dependence of APD in an Ad-CaM$_{1234}$ overexpressing myocyte. Fig. 2 *C* shows the plot of APD versus DI at different pacing rates (obtained from the same data in Fig. 2 *B*), yielding the dynamic APD restitution curve. The maximum slope of APD restitution was reduced to 0.8, compared to nontransfected or Ad-CaM$_{WT}$ overexpressing myocytes, whose maximum APD restitution slopes were 1.6 and 1.3, respectively. Note that at very long pacing CL, there was considerable beat-to-beat variability in APD; however, the APD variation was random rather than alternating. Fig. 3 summarizes the average data in each group.

To shorten APD back to control values (200–250 ms) in myocytes overexpressing Ad-CaM$_{1234}$, we added either 100 μM pinacidil or 10 μM verapamil to the superfusate (Fig. 2 *D*). Both pinacidil and verapamil restored APD to near normal, as shown graphically in Fig. 2 *E* and summarized in Fig. 3. During rapid pacing, seven of eight nontransfected myocytes developed APD alternans, at a pacing CL averaging 200 ms. In the example shown in Fig. 2 *E*, this is seen as the bifurcation in the black curve for CL $<$ 200 ms. In contrast, APD alternans was never observed in Ad-CaM$_{1234}$ overexpressing myocytes, either before or after exposure to pinacidil or verapamil (Fig. 2 *E* and Fig. 3 *B*). Fig. 2 *F* shows the dynamic APD restitution curves for these same myocytes, obtained by plotting APD versus DI using the same data in Fig. 2, *D* and *E*. After shortening APD in the Ad-CaM$_{1234}$ overexpressing myocytes using verapamil or pinacidil, APD restitution slope remained significantly <1 everywhere, compared to the nontransfected myocyte whose maximum APD restitution slope was 1.3. The summary data in Fig. 3 shows that APD restitution slope was reduced to <1 in all Ad-CaM$_{1234}$ overexpressing myocytes, both in the absence and presence of verapamil or pinacidil.

To study the effects of these interventions on contractility, we compared cell-shortening between nontransfected myocytes and Ad-CaM$_{1234}$-overexpressing myocytes treated with either pinacidil or verapamil. Pinacidil increased cell-shortening amplitude from 11 to 14%, whereas verapamil significantly depressed cell-shortening amplitude to 6% (Fig. 3 *B*).

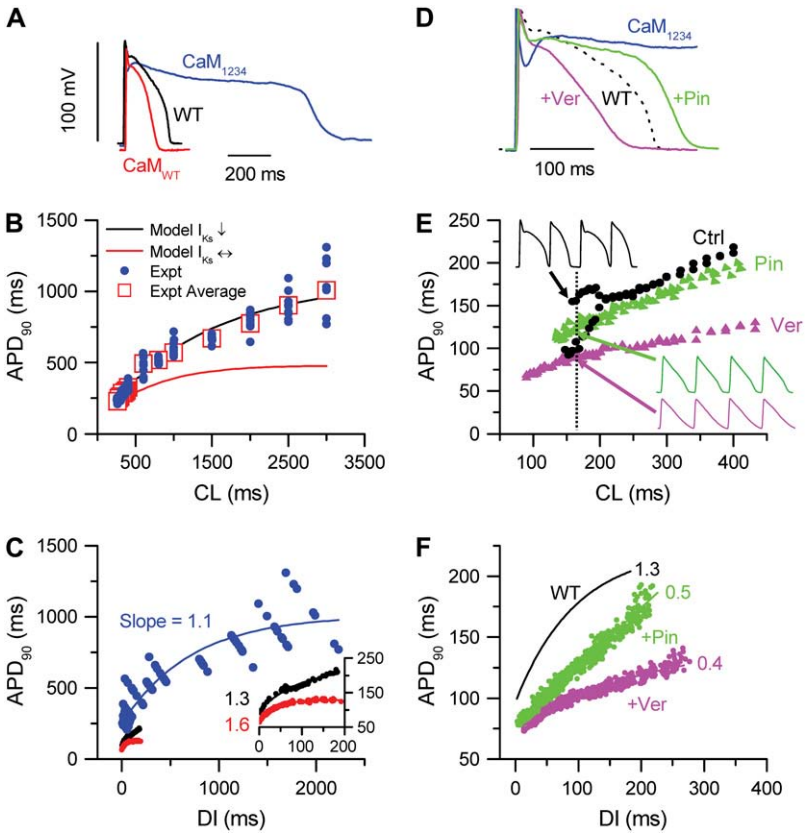

FIGURE 2 (*A*) Representative recordings of action potentials in current-clamped isolated rabbit ventricular myocytes transfected in vitro with either Ad-CaM$_{1234}$ (*blue*) or Ad-CaM$_{WT}$ (*red*), compared to a nontransfected (*black*) myocyte. (*B*) The rate dependence of APD in an Ad-CaM$_{1234}$ overexpressing myocyte, illustrating dramatic APD prolongation (and increased variability) at long pacing CL. Red boxes show the average at each CL. Solid lines shows the fits to the cell model simulating CaM$_{1234}$'s effects, assuming that I_{Ks} either is not (*red line* labeled *Model* I_{Ks} $\leftrightarrow$) or is also regulating by Ca-CaM (*blue line* labeled *Model* I_{Ks} $\downarrow$). (*C*) The dynamic APD restitution curve constructed from the data in panel *B*, illustrating that the maximum slope of APD restitution was reduced (0.8), in comparison to the nontransfected (*black*) or Ad-CaM$_{WT}$ overexpressing (*red*) myocyte (*inset*). (*D*) APD before (*blue*) and after 100 μM pinacidil (Pin, *green*) or 10 μM verapamil (Ver, *purple*) in myocytes overexpressing Ad-CaM$_{1234}$, compared to a nontransfected cell (WT, *black dots*). Since the traces were from different myocytes, the AP amplitudes were normalized for easier comparison of the APD. (*E* and *F*) The corresponding rate dependence of APD and dynamic APD restitution curves for the cases in panel *D*. Insets in panel *E* show representative AP recordings at the dashed vertical line for each case, illustrating the alternating APD (165 vs. 115 ms) in the nontransfected myocyte, and the lack of APD alternans (120 ms vs. 120 ms Pin; 90 ms vs. 90 ms Ver) in the transfected myocytes. Numbers in panel *F* indicate the maximal APD restitution slope. Experiments were conducted at 35–37°C using the perforated patch technique.

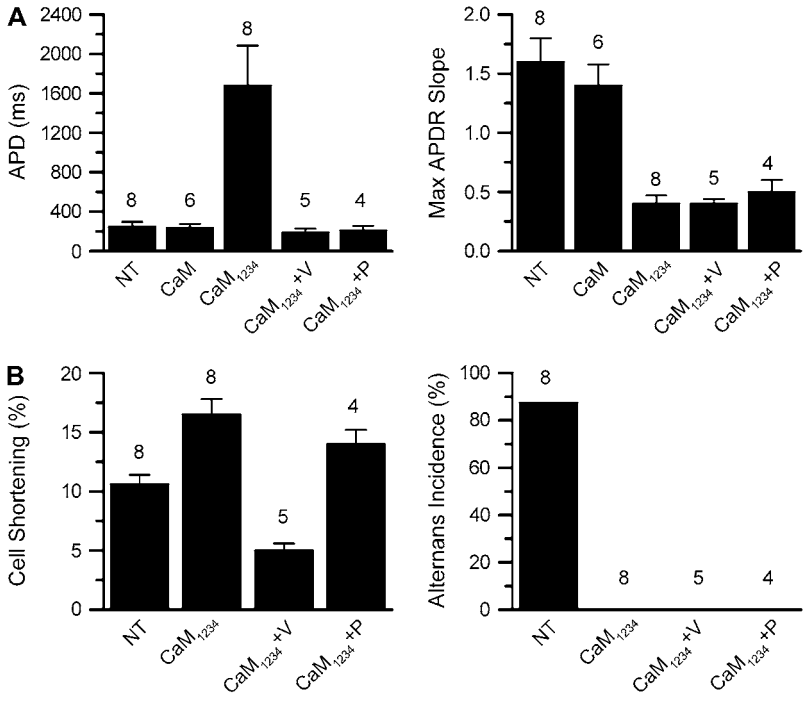

FIGURE 3 (*A*) Average data for APD (*left*) and maximal APD restitution (*APDR Slope*, *right*) for the number of myocytes indicated in the following groups: nontransfected (*NT*) or overexpressing CaM_{WT} (*CaM*), CaM_{1234} (*CaM_{1234}*), CaM_{1234} with 10 μmol/L verapamil (*CaM_{1234}+V*) added, and CaM_{1234} with 100 μmol/L pinacidil (*CaM_{1234}+P*) added. Pacing CL was 400 ms in all cases except CaM_{1234}, for was 3000 ms to illustrate the marked APD prolongation at long pacing CL. (*B*) The effects of pinacidil and verapamil on cell shortening (*left*) and the incidence of APD alternans (*right*) in Ad-CaM_{1234} overexpressing myocytes. Compared to nontransfected myocytes, pinacidil increased cell-shortening amplitude, whereas verapamil significantly depressed cell-shortening amplitude. Experiments were conducted at 37°C using the perforated patch technique.

These findings demonstrate that $I_{Ca,L}$ kinetics can be modified to flatten APD restitution slope and suppress APD alternans while independently regulating cell contractility, to either increase (with pinacidil) or decrease (with verapamil) cell shortening.

Simulating $I_{Ca,L}$ modification by Ad-CaM_{1234}

We first confirmed that the new AP model (12) accurately simulated the effects of Ca current blockers observed in real cardiac tissue (1,2,4). Fig. 4 *A* shows that blocking $I_{Ca,L}$ by 50% markedly suppressed the Ca_i transient during steady-state pacing at CL 250 ms. The marked suppression of the Ca_i transient was due to unloading of the SR (by 34% from 1.73 to 1.15 mmol/L) as a result of the reduced transsarcolemmal Ca influx via $I_{Ca,L}$, which also decreased the efficiency of $I_{Ca,L}$ at releasing SR Ca due to the highly nonlinear SR Ca release versus SR Ca load relationship (20). $I_{Ca,L}$ blockade also flattened both dynamic and S1S2 APD restitution curves, and prevented APD alternans during rapid pacing (Fig. 4 *A*). Note that dynamic and S1S2 APD restitution curves are not identical, due to the effects of short-term cardiac memory (i.e., APD is not a sole function of the previous DI, but also of the recent pacing history). Although the flatter APD restitution slope facilitated suppression of APD alternans, APD alternans in this model is more strongly driven by primary Ca_i alternans, consistent with experimental findings (4,21). For example, in the control cell model, the onset of alternans occurred at a DI of ~50 ms, at which the APD restitution slope was still <1 (Fig. 5 *D*). Primary Ca_i alternans depends strongly on the steepness of SR Ca release versus SR Ca load relationship (10,14), so that unloading of the SR by $I_{Ca,L}$ blockade also had a major influence on suppressing primary Ca_i alternans, thereby suppressing APD alternans secondarily.

When a spiral wave was initiated in homogeneous two-dimensional simulated tissue (7.5 cm × 7.5 cm) using the control cell AP model, the spiral wave spontaneously broke up into multiple wavelets resembling fibrillation (Fig. 4 *B*). After blocking $I_{Ca,L}$ by 50%, however, the spiral wave remained intact (Fig. 4 *C*), with the tip trajectory tracing quasiperiodic meander (the *flower petal pattern* expanded in the *last panel*). These findings demonstrate that the dynamic AP model replicates experimental results obtained using D600 to block $I_{Ca,L}$ in rabbit ventricle (2), and verapamil in canine ventricles (1).

To simulate the effects of CaM_{1234}, we assumed that Ad-CaM_{1234} overexpression resulted in two populations of L-type Ca channels: a fraction (α) in which CaM_{1234} replaced the native wild-type CaM normally tethered to the channel, and a fraction (1-α), which remained associated with native CaM. We assumed that the α fraction exhibited only VDI, whereas the (1-α) fraction exhibited both CDI and VDI. Fig. 5 *A* shows that when α was increased in steps from zero to a maximum of 0.6, the remaining noninactivated $I_{Ca,L}$ pedestal current at the end of a 300-ms square voltage-clamp pulse to +10 mV progressively increased from ~10% to ~40%, since a larger fraction of channels did not undergo CDI. This result covers the range in myocytes infected with Ad-CaM_{1234}, where the pedestal current averaged ~40% of the peak (Fig. 1 *C*).

When this modification was incorporated into the AP model, the steady-state APD at a pacing CL of 400 ms

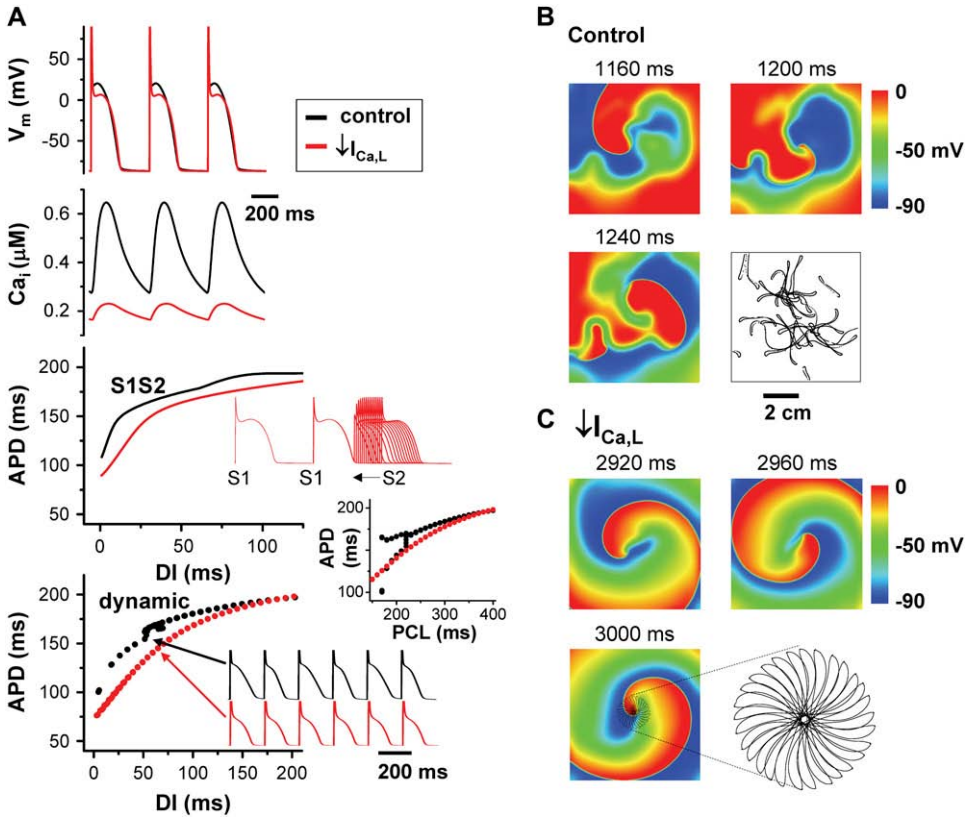

FIGURE 4 Dependence of spiral wave dynamics on $I_{Ca,L}$ current density in the AP model. (*A*) Comparison of APs (*upper panel*), Ca_i transients (*second panel*), S1S2 restitution curves (*third panel*), and dynamic pacing curves (*lower panel*) for control parameters (*black traces*) and when $I_{Ca,L}$ has been decreased by 50% in the AP model (*red traces*). With $I_{Ca,L}$ blockade, the steady-state APD is not much affected at this CL, but the Ca_i transient is markedly suppressed. The S1S2 APD restitution slope (*inset* illustrates the pacing protocol) is shallower than in control, as is the dynamic APD restitution slope (*lower panel*), and APD alternans is completely eliminated (*lower panel inset*, APD = 166 vs. 143 ms for control and 140 vs. 140 ms for $I_{Ca,L}$ blockade). (*B*) Voltage snapshots at the times indicated after initiation of spiral wave reentry under control conditions. The spiral wave breaks up into multiple wavelets. Membrane voltage scale is indicated by the color bar. Last panel shows the complex trajectory of the multiple spiral wave tips. (*C*) After $I_{Ca,L}$ reduction, the spiral wave is stable. The core of the spiral wave undergoes stable quasiperiodic meander, as shown in the expanded tip trajectory in the last panel.

prolonged modestly from 199 ms to 276 ms with $\alpha = 0.3$. However, in contrast to experimental observations, even at long CL, APD did not prolong markedly (*red line* in Fig. 2 *B*), even for $\alpha = 0.6$. To accurately simulate APD at long CL required blocking I_{Ks}, which is now known also to be regulated by CaM (22,23), and therefore is also expected to be suppressed by CaM_{1234} overexpression. After reducing I_{Ks} by 60%, the CL dependence of APD matched the experimental findings, as shown in the blue traces for $\alpha = 0.3$ in Figs. 2 *B* and 5 *B*. Fig. 5 *C* (*blue trace*) shows the corresponding Ca_i transient for the AP paced at 3000 ms CL (*dashed blue trace*). The very long APD at the slow pacing rate had a small Ca_i transient, due to SR unloading during the long diastolic interval. However, at 400 ms CL, both diastolic and systolic Ca_i were markedly elevated due to the enhanced systolic Ca influx through the noninactivating component of $I_{Ca,L}$ and the short DI. This effect became more prominent as α was further increased. To simulate shortening APD back to the control level by pinacidil, we activated I_{KATP}. Although I_{KATP} activation successfully shortened APD with $\alpha = 0.3$ back to the control value (*green trace* in Fig. 5 *B*), this intervention did not return the corresponding Ca_i transient amplitude at 400 ms CL (*green trace* in Fig. 5 *C*) to normal, since transsarcolemmal Ca entry via $I_{Ca,L}$ was still substantially increased by the absence of CDI in a significant fraction of the L-type Ca channels. This is consistent with the experimental finding that pinacidil increased cell shortening in CaM_{1234} overexpressing myocytes (Fig. 3 *B*). In contrast, if APD was shortened by reducing the maximal conductance of L-type Ca channels ($G_{Ca,L}$) by 69% to simulate the effects of verapamil (*purple trace* in Fig. 5 *B*), the Ca_i transient was significantly suppressed (*purple trace* in Fig. 5 *C*), as was observed experimentally (Fig. 3 *B*). For $\alpha < 0.4$, a combined intervention of modestly increasing I_{KATP} and reducing $G_{Ca,L}$ (by 34%) could shorten APD to the normal range while maintaining a normal Ca_i transient amplitude (*red trace* in Fig. 5, *B* and *C*). For $\alpha = 0.4$ or greater, however, it was not possible to maintain both a normal APD and Ca_i transient amplitude during pacing at 400 ms by dually adjusting $G_{Ca,L}$ and I_{KATP}—i.e., if APD was normal, the Ca_i transient was supernormal, and if the Ca_i transient was normal, the APD was significantly abbreviated.

Hereafter, we refer to these combined $I_{Ca,L}$ modifications (with $\alpha = 0.3$ so as to maintain both normal APD and Ca_i transient) as the CaM_{1234}+P+V cell model. Note that the Ca_i transient peaks later in the CaM_{1234}+P+V cell compared to the control cell. This reflects the fact that during steady-state pacing at a CL of 400 ms in the control cell model, more SR Ca release occurs during the early phase of the AP when the $I_{Ca,L}$ reaches its peak, whereas in the CaM_{1234}+P+V, SR Ca release is triggered more gradually

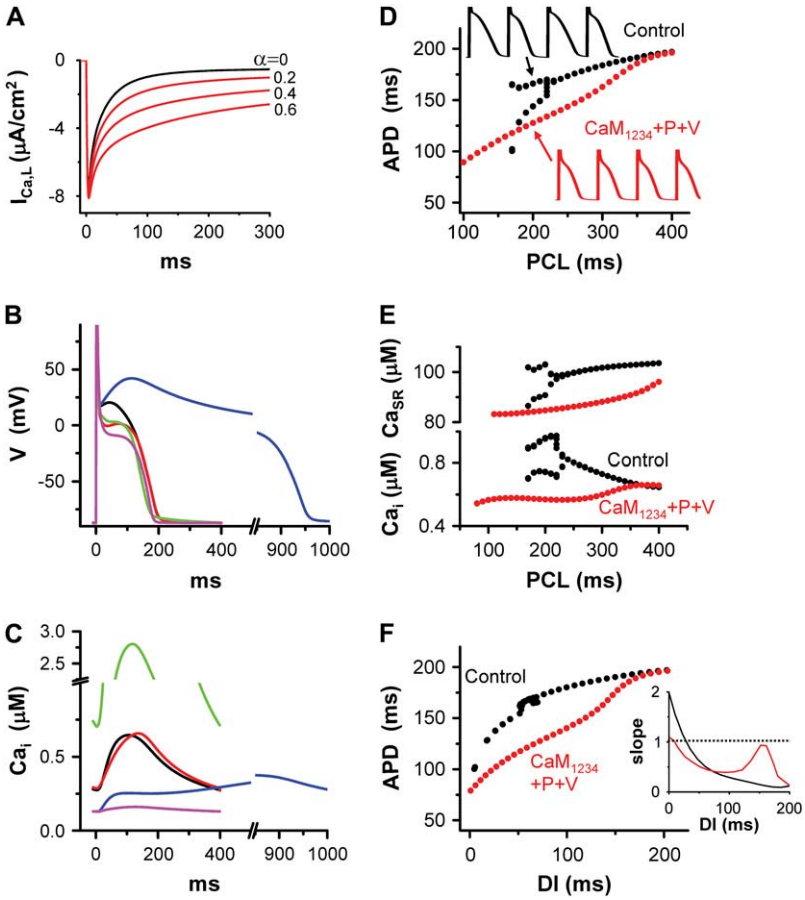

FIGURE 5 Effects of suppressing Ca-induced inactivation of $I_{Ca,L}$ in the AP model. To simulate CaM_{1234} overexpression, the fraction of channels α exhibiting VDI but not CDI was varied from 0.2 to 0.6. (*A*) Simulated current traces corresponding to $I_{Ca,L}$ during a 300 ms voltage-clamp from –80 to 0 mV, for the control (*black*, $\alpha = 0$) and CaM_{1234} (*red*, α as labeled) cell models. (*B*) Steady-state action potential morphology during pacing at 400 ms PCL, simulating the following conditions: Control (*black trace*), CaM_{1234} (*blue*), CaM_{1234}+ Pinacidil (CaM_{1234}+ P, *green trace*), and CaM_{1234}+ Pinacidil + Verapamil (CaM_{1234}+ P+V, *red*), where CaM_{1234} corresponds to $\alpha = 0.3$, Pinacidil to $g_{katp} = 0.663$ mS/μF, and Verapamil to $g_{ca} = 120$ mmol/(cm *C*). (*C*) Corresponding Ca_i transients for the same conditions. (*D* and *E*) Rate-dependent properties of APD, end diastolic SR Ca content (Ca_{SR}), and Ca_i transient amplitude during steady-state pacing from 400 ms to the onset of 2:1 block, for the control (*black*) and CaM_{1234}+P+V (*red*) cell models. Insets in panel *D* show AP traces during pacing at the cycle length (PCL) indicated by the arrows, demonstrating elimination of APD alternans (APD 166 ms vs. 143 ms for control, 128 ms vs. 128 ms for the CaM_{1234}+P+V model). (*F*) Dynamic APD restitution curve obtained from the same data set in panel *D*. APD restitution slope versus DI curve is shown in the inset (*dashed line* indicates slope = 1.0).

throughout the AP. In both cases, the components of the Ca transient arising from $I_{Ca,L}$ and SR were similar (20% and 80%, respectively, for the control cell model, and 19% and 81%, respectively, for the CaM_{1234}+P+V cell), indicating that the fundamental balance between transsarcolemmal Ca movement and SR Ca recycling were not significantly perturbed from the normal state.

Fig. 5, *D* and *E*, compare the rate dependence of APD and peak Ca_i transient amplitude during a dynamic pacing protocol where the pacing CL was decreased by 2 ms every 10 beats (to mimic the experimental myocyte protocol), starting from 400 ms. APD and peak Ca_i transient amplitude were plotted for the 10th beat at each pacing CL. In the normal cell model, the onset of APD and Ca_i transient alternans occurred at a pacing CL of 220 ms. In the CaM_{1234}+P+V cell model, however, alternans was abolished. Moreover, the Ca_i transient amplitude decreased in the CaM_{1234}+P+V cell model as pacing CL shortened, protecting against Ca_i overload at very fast heart rates. Fig. 5 *F* compares the corresponding dynamic APD restitution curves obtained by plotting APD versus DI for the same data in Fig. 5 *D*. The maximum APD restitution slope was reduced from 2.1 in the control cell model to <1 everywhere in the CaM_{1234}+P+V cell model, similar to the myocyte experiments. Similar results were obtained for other values of α ranging from 0.2 to 0.6, in which $G_{Ca,L}$ and I_{KATP} were adjusted to keep the Ca_i transient amplitude normal. The flattening of APD restitution slope and suppression of alternans was due to the modification of $I_{Ca,L}$ rather than I_{Ks}, since blocking I_{Ks} without modifying $I_{Ca,L}$ steepened APD restitution slope and promoted alternans. Conversely, modifying $I_{Ca,L}$ without blocking I_{Ks} still flattened APD restitution slope and prevented alternans.

Although the flatter APD restitution slope in the CaM_{1234}+P+V cell model is expected to suppress APD alternans, as noted earlier, APD alternans in this model is more strongly driven by primary Ca_i alternans. Thus, to prevent APD and Ca_i transient alternans, the $I_{Ca,L}$ modifications in the CaM_{1234}+P+V cell model must also have favorably influenced Ca_i cycling stability. This was due in part (see Discussion) to a decrease in the SR Ca load in the CaM_{1234}+P+V cell as pacing CL decreased below 400 ms, since Ca_i transient alternans is highly sensitive to the SR Ca load (14). In contrast, for the control cell, the Ca_i transient and SR Ca load progressively increased as pacing CL decreased below 400 ms (Fig. 5 *E*). This effect was seen for all values of α between 0.2 and 0.6 in which $G_{Ca,L}$ and I_{KATP} were adjusted to keep the Ca_i transient amplitude normal.

Effects of $I_{Ca,L}$ modification on APD alternans and spiral wave breakup in simulated cardiac tissue

We next examined how $I_{Ca,L}$ modification in the CaM_{1234}+P+V cell model affected arrhythmogenesis in simulated cardiac tissue. Fig. 6 *A* shows the effects of rapid pacing in a one-dimensional cable. For the control cell model, spatially discordant alternans developed at a pacing CL of 180 ms. The black and blue lines shows the APD distribution along a 4.5 cm cable for two successive beats. For the CaM_{1234}+P+V cell model (*red line*), however, no APD alternans developed at the fastest pacing CL, precluding the development of spatially discordant alternans. Similarly, in two-dimensional tissue, spatially discordant alternans of both APD and the Ca_i transient developed when the control cell model was paced at 180 ms. Fig. 6 *B* (*upper panel*) shows the gradients in APD (*upper panels*) and Ca_i transient amplitude (*lower panels*) for two successive beats during pacing at a CL of 180 ms in a 4.5 cm × 4.5 cm tissue (*upper panel*). Nodal lines, where alternans amplitude is zero, separate the out-of-phase regions of APD and Ca_i transient alternans. In two-dimensional tissue composed of CaM_{1234}+P+V cells, however, APD shortened more quickly as the pacing rate increased, alternans was suppressed, and therefore no spatially discordant APD or Ca_i transient alternans occurred either (Fig. 6 *C*).

Fig. 7 shows membrane voltage snapshots during spiral wave reentry in a large (7.5 cm × 7.5 cm) tissue consisting of coupled CaM_{1234}+P+V cells with $\alpha = 0.3$. As for the case when $I_{Ca,L}$ was blocked by 50% (Fig. 4 *C*), the spiral wave remained intact, with the tip trajectory exhibiting quasiperiodic meander (*flower petal pattern*). In contrast, the control cell model broke up into multiple wavelet fibrillation, as shown in Fig. 4 *B*. Spiral wave breakup was prevented for other values of α ranging from 0.2 to 0.6, as long as $G_{Ca,L}$ and I_{KATP} were adjusted to keep the Ca_i transient amplitude normal during pacing at 400 ms CL.

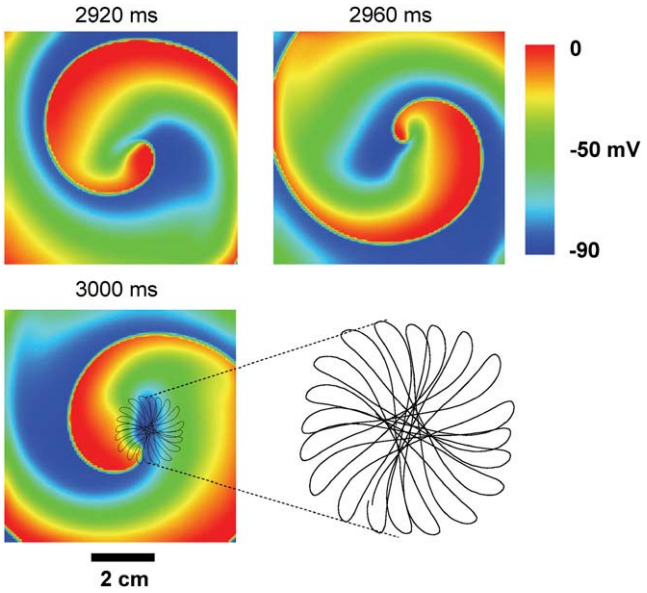

FIGURE 7 Voltage snapshots of spiral wave reentry in simulated two-dimensional tissue using the CaM_{1234}+P+V cell model. The spiral wave, initiated at 0 ms, remains intact. The last panel shows magnified trajectory of the spiral tip, demonstrating quasiperiodic meander. Membrane voltage scale is indicated by the color bar.

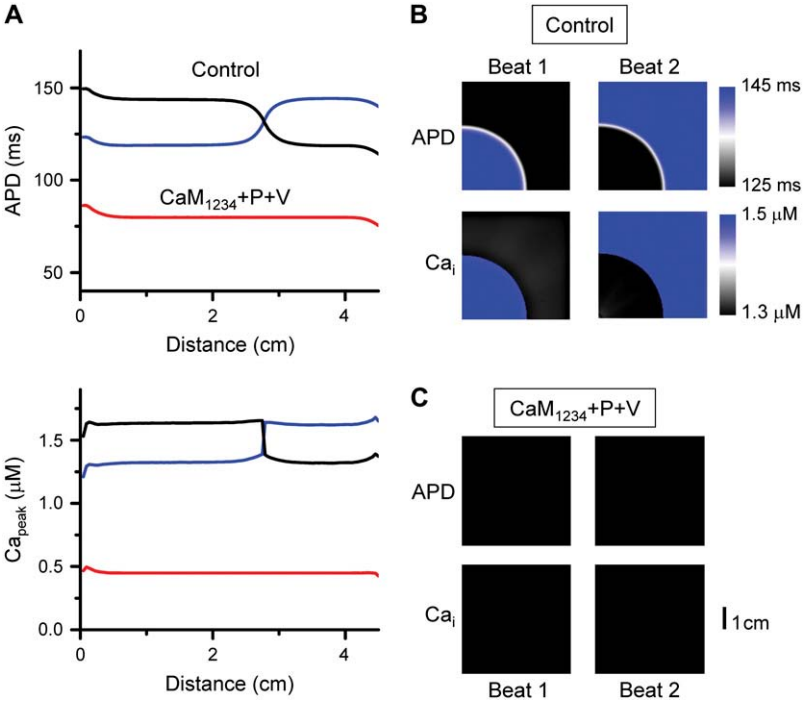

FIGURE 6 (*A*) Spatially discordant alternans in a one-dimensional cable (4.5 cm) paced from the left end. The control cell model exhibits discordant alternans at a pacing CL = 180 ms. The blue and black line shows the APD distribution along the cable for two alternate beats at that pacing rate. Crossing of the lines indicates a node where the alternans amplitude is zero. The red line shows the APD for two successive beats for the CaM_{1234}+P+V cell model at the fastest pacing CL before 2:1 block, which, like all other pacing CL, failed to develop APD or Ca_i alternans. (*B*) Spatially discordant alternans in APD and Ca_i transient amplitude in homogeneous two-dimensional tissue (4.5 cm × 4.5 cm) during pacing CL = 180 ms for the control cell model. The panels show the spatial distributions of APD (*above*) and Ca_i transient amplitude (*below*) for two successive beats, demonstrating two regions alternating out-of-phase with each other, separated by a nodal line (*white*) without alternans. (*C*) Same for the CaM_{1234} cell model, demonstrating the lack of spatially discordant alternans, even at the shortest pacing CL.

These simulations predict that to suppress alternans and fibrillation while maintaining a normal APD and Ca_i transient, the ideal therapeutic window for the CaM_{1234}+P+V modification occurs for $\alpha = 0.2$–0.4, i.e., with 20–40% of L-type Ca channels modified by CaM_{1234} to prevent CDI. The prevention of spatially discordant alternans and spiral wave breakup was due to the modification of $I_{Ca,L}$ rather than I_{Ks}, since blocking I_{Ks} without modifying $I_{Ca,L}$ neither prevented spatially discordant alternans nor spiral wave breakup, whereas modifying $I_{Ca,L}$ without blocking I_{Ks} did.

DISCUSSION

In this study we overexpressed mutant Ca-insensitive calmodulin CaM_{1234} in isolated rabbit ventricular myocytes to examine the influence of altering $I_{Ca,L}$ inactivation kinetics during the cardiac AP on excitation-contraction coupling and repolarization. A major goal was to test the hypothesis that $I_{Ca,L}$ kinetics can be modified to increase dynamic wave stability, by flattening APD restitution slope and preventing APD and Ca_i transient alternans, without decreasing contractility. Experimentally, we showed that these goals could be achieved when CaM_{1234} overexpression to inhibit CDI was combined with activation of I_{KATP} by the drug pinacidil to prevent excessive APD prolongation.

To investigate the underlying mechanisms, we used a new rabbit ventricular AP cell model that contains a Markovian formulation of $I_{Ca,L}$ to explicitly represent the CDI and VDI components inactivation, and also incorporates a dynamic model of Ca_i cycling capable of generating Ca_i transient alternans (12). Although previous experimental studies have documented that $I_{Ca,L}$ blockade flattens APD restitution slope, suppresses cardiac alternans, and prevents VF by inhibiting breakup of reentrant waves (1,2,4), none of the currently available latest generation AP models reproduces all of these effects. With the improvements introduced into the new rabbit ventricular model, however, all of the experimentally observed effects of Ca channel blockade on APD restitution, APD, and Ca_i alternans were replicated (Fig. 4). The model simulated the experimental results of CaM_{1234} interventions confirming the reliability of the model's predictions and providing further insights into the mechanisms leading to dynamic wave stability. This approach provides a novel paradigm illustrating the usefulness of combined experimental and modeling studies for characterizing drugs or gene products that influence ion channel kinetics.

Effects of $I_{Ca,L}$ modification on APD and Ca_i transient amplitude

From the simulations, we gained insight into the roles played by early and late phases of $I_{Ca,L}$ during the cardiac AP. The early phase of $I_{Ca,L}$ is more important for regulating SR Ca release, while the latter phase influences both repolarization and SR Ca loading. Thus, if the early peak of $I_{Ca,L}$ is preserved when CDI is inhibited by CaM_{1234}, the cell becomes markedly Ca-overloaded due to increased transsarcolemmal Ca influx during the late phase of the AP, and APD is prolonged by the persistent inward current (11). However, the degree of APD prolongation was relatively modest (even for $\alpha = 0.6$), especially at long pacing CL, if the CaM_{1234} suppression of I_{Ks} was not also taken into account (23,24). Our simulations suggest that acute regulation of $I_{Ca,L}$ and I_{Ks} by CaM may both be important in preventing ultralong action potentials observed at slow heart rates.

If APD prolongation by CaM_{1234} overexpression is reversed by increasing an outward current such as I_{KATP}, APD becomes normal, but transsarcolemmal Ca influx during the late AP is still greatly increased, promoting Ca_i overload. Alternatively, if APD is normalized by partially blocking $I_{Ca,L}$, the reduction in the early peak of $I_{Ca,L}$ disproportionately suppresses SR Ca release. In this case, APD becomes normal, but the Ca_i transient peak is depressed and delayed. To achieve both a normal APD and normal Ca_i transient required a combination I_{KATP} activation and $I_{Ca,L}$ blockade, such that the reduction of early SR Ca release was offset by the greater transsarcolemmal Ca influx during the latter part of the AP, leading to normal amplitude Ca_i transient with a modestly delayed time-to-peak. It is noteworthy that only a modest blockade (34%) of $I_{Ca,L}$ was required to achieve this effect. Consistent with these findings, we found that in isolated myocytes overexpressing CaM_{1234}, verapamil could restore APD to normal, but in doing so also significantly suppressed cell shortening (Fig. 3). In contrast, when pinacidil was used to restore APD, cell shortening was increased (Fig. 3). Simulations agreed with these observations, although the increase in Ca_i observed experimentally with pinacidil was not as extreme as predicted in the simulations (Fig. 5 *C*). Thus, some compensatory mechanism must come into play to protect the real myocytes from extreme Ca_i overload and cell death. Peak $I_{Ca,L}$ was not reduced in isolated myocytes overexpressing CaM_{1234}, so other, as yet unidentified mechanisms, may come into play.

The proper balance of I_{KATP} activation and $I_{Ca,L}$ blockade to maintain both normal APD and Ca_i transient amplitude during pacing at 400 ms was only achievable for $\alpha < 0.4$. For $\alpha = 0.4$ or greater, if APD was normal, the Ca_i transient was too large, and if the Ca_i transient was normal, APD was too short. These results suggest that the ideal therapeutic target is modification of no more than 40% of L-type Ca channels by CaM_{1234}.

Effects of $I_{Ca,L}$ modification on APD restitution, APD and Ca_i alternans and dynamic wave stability

APD restitution slope is regulated by the recovery from inactivation of inward currents, deactivation of outward currents, and restitution of the Ca_i transient through its influence on Ca-sensitive plateau currents such as the Na-Ca

exchange current. The range of DI (0–50 ms) over which APD restitution is steepest corresponds to the time constants of recovery from inactivation of I_{Na} between 0 and 10 ms, and $I_{Ca,L}$ between 10 and 50 ms (3). In the case of $I_{Ca,L}$, its effect on APD restitution slope is mediated by both recovery from inactivation and $I_{Ca,L}$ amplitude during the late phase of the AP. When peak $I_{Ca,L}$ amplitude is reduced by a Ca channel blocker such as verapamil, SR Ca load decreases, which suppresses the Ca_i transient (Fig. 5 *C*), so that $I_{Ca,L}$ inactivation by CDI is reduced. With less inactivation to recover from, the influence of $I_{Ca,L}$ recovery of APD at short DI is diminished, resulting in a flatter APD restitution slope over this DI range. Through inhibiting inactivation, CaM_{1234} also decreased APD restitution slope by this mechanism, even though peak $I_{Ca,L}$ remained normal. For example, in the control AP model, when DI increased from 10 to 50 ms, peak $I_{Ca,L}$ increased from 3.9 to 5.4 pA/pF and APD by 40 ms from 110 to 150 ms (Fig. 5 *F*). In the case of CaM_{1234} +P+V, however, the same change in DI from 10 to 50 ms was associated with a lesser increase in peak $I_{Ca,L}$ from 3.5 to 4.7, and the change in APD was also less (88 to 117 ms), producing a flatter APD restitution slope.

Recent evidence indicates that the onset of APD alternans during rapid pacing occurs primarily as a result of a Ca_i-cycling instability, rather than steep APD restitution slope (4,21). Theoretical analysis (10,14) has shown that this Ca_i-cycling instability results from a steep dependence of fractional SR Ca release on SR Ca load, coupled with a time delay in availability of the SR Ca release (either ryanodine receptor recovery or a transport delay from SR uptake sites to SR release sites). Ca channel blockade causing decreased Ca entry is expected to prevent APD alternans by both mechanisms, i.e., by flattening the APD restitution slope as well as by unloading the SR. Although CaM_{1234} +P+V flattened the APD restitution slope, which tends to suppress APD alternans, its effects on the Ca_i-cycling instability were not intuitively obvious, since the Ca_i transient remained normal during pacing at 400 ms CL. However, the CaM_{1234}+P+V cell model provided a plausible mechanistic explanation, since SR Ca content fell progressively as pacing CL was further shortened (Fig. 5 *E*). Thus, in the control cell model, in which most SR Ca release is triggered during the early phase of the AP (since $I_{Ca,L}$ is largely inactivated by CDI during the late phase), the SR stops releasing and begins to reaccumulate Ca during the late phase of the AP. In the CaM_{1234}+P+V cell model, however, incomplete $I_{Ca,L}$ inactivation during the late phase of the AP causes the SR to continue releasing Ca, so that the SR cannot effectively reaccumulate Ca until repolarization, when electrogenic Na-Ca exchange can compete much more effectively to extrude Ca from the cell. At lower SR Ca content, the dependence of fractional SR Ca release on SR Ca load is less steep, protecting against Ca_i alternans. Evidence for continued SR Ca release during the later phases of the AP is also manifest in the CaM_{1234}+P+V cell model by the delayed peak in the Ca_i transient relative to the control cell model (Fig. 5 *C*). Although this prediction of the model needs to be experimentally validated in real myocytes, it illustrates how modeling can reveal nonintuitive insights into the mechanism. An additional factor suppressing Ca_i alternans arises from the positive coupling between the Ca_i transient and APD, which is electromechanically concordant (i.e., a large Ca_i transient promotes a long APD and vice versa) in both the control cell and CaM_{1234}+P+V cell models. In a detailed analysis of the coupling relationships between APD and Ca_i in cardiac cells, Shiferaw et al. (24) showed that if the coupling between APD and Ca is positive, then flattening the APD restitution curve suppresses alternans, even though Ca_i cycling dominates the underlying alternans instability. Thus, the flatter APD restitution slope in the CaM_{1234} +P+V cell model in the setting of positive coupling also is predicted to contribute to the suppression of alternans.

The effects of flattening APD restitution and preventing APD and Ca_i alternans in the CaM_{1234}+P+V cell model at the cellular scale also suppressed the formation of spatially discordant alternans during rapid pacing at the tissue scale in simulated one-dimensional and two-dimensional homogeneous tissue. In two-dimensional tissue, the CaM_{1234}+P+V cell model prevented spiral wave breakup, but did not suppress the spiral wave tip from meandering in a quasi-periodic pattern (Fig. 7). This may be desirable as an antiarrhythmic strategy, since spiral/scroll wave tip meander increases the chance that the spiral/scroll wave will collide with a tissue border and self-terminate (25).

Implications and limitations

These findings highlight the importance of $I_{Ca,L}$ as sitting at a focal point regulating cardiac action potential duration, excitation-contraction coupling, and dynamic wave stability relevant to arrhythmogenesis. Not only does $I_{Ca,L}$ regulate APD through APD restitution, but it also plays a major role, along with Na-Ca exchange, in mediating the effects of the Ca_i transient on APD. This interplay between APD and Ca_i cycling instabilities produces a rich dynamical repertoire influencing wave stability (24,26). Although the implications of this study for novel antiarrhythmic drug development are very preliminary, they nevertheless highlight the potential usefulness of physiologically realistic computer modeling to design and test in silico novel therapeutic approaches, which, if promising, can then be tested experimentally.

With respect to our findings, there are a number of important limitations. Even though we documented that gene transfer of Ad-CaM_{1234} into isolated rabbit ventricular myocytes was effective at flattening APD restitution slope and APD alternans, we currently are limited in our ability to achieve sufficiently homogenous gene expression in vivo throughout the ventricles to test whether the $I_{Ca,L}$ modification strategy favorably influenced arrhythmogenesis, as predicted by the simulations. This will have to await further improvements in gene delivery technology. For gene-targeted antiarrhythmic

therapy, homogeneous gene expression is a particularly critical issue, since heterogeneous gene expression on a scale larger than the electrical space constant of 1–2 mm may enhance electrophysiological dispersion, which is proarrhythmic. In addition, although useful as a proof-of-concept test, CaM_{1234} is not feasible for clinical antiarrhythmic applications, because it interferes with Ca-CaM signaling regulating other vital cellular processes. Moreover, although reducing CDI by CaM_{1234} overexpression flattened APD restitution and suppressed alternans, it also prolonged APD markedly at slow heart rates, putatively by suppressing I_{Ks} (22,23), which had to be compensated by activating I_{KATP} or partially blocking $I_{Ca,L}$. Clinical application would require that this delicate balance be maintained over a wide range of physiological conditions to avoid excessive APD prolongation leading to long QT syndrome and its associated proarrhythrogenic consequences including afterdepolarizations, triggered activity, and torsades de pointes. Given the significant degree of regional electrophysiological heterogeneity in normal heart, this delicate balance may not be achievable, especially when disease-related remodeling further increases tissue heterogeneity. For example, Timothy Syndrome is a genetic channelopathy in which defective $I_{Ca,L}$ inactivation causes QT prolongation and increased risk of sudden cardiac death (27). Our findings suggest that normalization of the QT interval in these patients with drugs such as K channel openers or $I_{Ca,L}$ blockers may be an effective therapy, since they are predicted to enhance dynamic wave stability by flattening APD restitution slope and suppressing APD and Ca_i alternans.

Rather than inhibiting $I_{Ca,L}$ inactivation, a potentially superior way to modify $I_{Ca,L}$ to prevent arrhythmias might be to accelerate $I_{Ca,L}$ inactivation, so that the early peak $I_{Ca,L}$ essential for triggering normal SR Ca release is preserved, but the effects of late $I_{Ca,L}$ on repolarization are diminished. We are currently investigating this possibility in our model, although we are not currently aware of any drug or gene product that could be used to test this idea experimentally in cardiac myocytes. Ancillary $I_{Ca,L}$ subunits, particularly the large family of β-subunits, have a strong influence on $I_{Ca,L}$ inactivation kinetics and possibly can exert the desired effect. Unlike CaM_{1234}, overexpression of ancillary Ca channel subunits has the potential as a highly selective method to modify $I_{Ca,L}$ kinetics.

Finally, the usefulness of enhancing dynamic wave stability as an antiarrhythmic strategy is still unproven, especially in the setting of diseased hearts. Although suppression of alternans is antiarrhythmic, by stabilizing rotors, enhanced dynamic wave stability also reduces their meander and chance of self-terminating by colliding with a tissue border (25), potentially converting a nonsustained nonlethal arrhythmia into a sustained lethal arrhythmia. Our simulations showed that the $I_{Ca,L}$ modification strategy we simulated prevented spiral wave breakup in two-dimensional tissue, but preserved spiral wave meander, which increases the likelihood of self-termination (25).

In summary, despite these limitations, our findings suggest that $I_{Ca,L}$ modification as an antifibrillatory therapy deserves further investigation.

This research benefited from fruitful exchanges that took place at the Cardiac Dynamics program hosted in 2007 by the Kavli Institute for Theoretical Physics at the University of California, Santa Barbara.

This research was supported by National Institutes of Health/National Heart, Lung, and Blood Institute grants No. P50 HL53219 and No. P01 HL078931, the Laubisch and Kawata Endowments, the University of California at Los Angeles STAR Fellowship Program, and the Sarnoff Cardiovascular Research Foundation.

REFERENCES

1. Riccio, M. L., M. L. Koller, and R. F. Gilmour, Jr. 1999. Electrical restitution and spatiotemporal organization during ventricular fibrillation. *Circ. Res.* 84:955–963.
2. Wu, T. J., S. F. Lin, J. N. Weiss, C. T. Ting, and P. S. Chen. 2002. Two types of ventricular fibrillation in isolated rabbit hearts: importance of excitability and action potential duration restitution. *Circulation.* 106: 1859–1866.
3. Qu, Z., J. N. Weiss, and A. Garfinkel. 1999. Cardiac electrical restitution properties and stability of reentrant spiral waves: a simulation study. *Am. J. Physiol.* 45:H269–H283.
4. Goldhaber, J. I., L. H. Xie, T. Duong, C. Motter, K. Khuu, and J. N. Weiss. 2005. Action potential duration restitution and alternans in rabbit ventricular myocytes: the key role of intracellular calcium cycling. *Circ. Res.* 96:459–466.
5. Pastore, J. M., S. D. Girouard, K. R. Laurita, F. G. Akar, and D. S. Rosenbaum. 1999. Mechanism linking T-wave alternans to the genesis of cardiac fibrillation. *Circulation.* 99:1385–1394.
6. Qu, Z., A. Garfinkel, P. S. Chen, and J. N. Weiss. 2000. Mechanisms of discordant alternans and induction of reentry in simulated cardiac tissue. *Circulation.* 102:1664–1670.
7. Watanabe, M. A., F. H. Fenton, S. J. Evans, H. M. Hastings, and A. Karma. 2001. Mechanisms for discordant alternans. *J. Cardiovasc. Electrophysiol.* 12:196–206.
8. Soldatov, N. M. 2003. Ca channel moving tail: link between Ca-induced inactivation and Ca^{2+} signal transduction. *Trends Pharmacol. Sci.* 24:167–171.
9. Cens, T., M. Rousset, J. P. Leyris, P. Fesquet, and P. Charnet. 2006. Voltage- and calcium-dependent inactivation in high voltage-gated Ca channels. *Prog. Biophys. Mol. Biol.* 90:104–117.
10. Weiss, J. N., A. Karma, Y. Shiferaw, P. S. Chen, A. Garfinkel, and Z. Qu. 2006. From pulsus to pulseless: the saga of cardiac alternans. *Circ. Res.* 98:1244–1253.
11. Alseikhan, B. A., C. D. DeMaria, H. M. Colecraft, and D. T. Yue. 2002. Engineered calmodulins reveal the unexpected eminence of Ca channel inactivation in controlling heart excitation. *Proc. Natl. Acad. Sci. USA.* 99:17185–17190.
12. Mahajan, A., Y. Shiferaw, D. Sato, A. Baher, R. Olcese, L.-H. Xie, M.-J. Yang, P.-S. Chen, J. G. Restrepo, A. Karma, A. Garfinkel, Z. Qu, and J. N. Weiss. 2007. A rabbit ventricular action potential model replicating cardiac dynamics at rapid heart rates. *Biophys. J.* 94:392–410.
13. Shannon, T. R., F. Wang, J. Puglisi, C. Weber, and D. M. Bers. 2004. A mathematical treatment of integrated Ca dynamics within the ventricular myocyte. *Biophys. J.* 87:3351–3371.
14. Shiferaw, Y., M. A. Watanabe, A. Garfinkel, J. N. Weiss, and A. Karma. 2003. Model of intracellular calcium cycling in ventricular myocytes. *Biophys. J.* 85:3666–3686.
15. Goldhaber, J. I., J. M. Parker, and J. N. Weiss. 1991. Mechanisms of excitation-contraction coupling failure during metabolic inhibition in guinea-pig ventricular myocytes. *J. Physiol.* 443:371–386.

16. Rae, J., K. Cooper, P. Gates, and M. Watsky. 1991. Low access resistance perforated patch recordings using amphotericin B. *J. Neurosci. Methods*. 37:15–26.

17. Arena, J. P., and R. S. Kass. 1989. Activation of ATP-sensitive K channels in heart cells by pinacidil: dependence on ATP. *Am. J. Physiol.* 257:H2092–H2096.

18. Shaw, R. M., and Y. Rudy. 1997. Electrophysiologic effects of acute myocardial ischemia: a mechanistic investigation of action potential conduction and conduction failure. *Circ. Res.* 80:124–138.

19. Qu, Z. 2006. Critical mass hypothesis revisited: role of dynamical wave stability in spontaneous termination of cardiac fibrillation. *Am. J. Physiol.* 290:H255–H263.

20. Bassani, J. W., W. Yuan, and D. M. Bers. 1995. Fractional SR Ca release is regulated by trigger Ca and SR Ca content in cardiac myocytes. *Am. J. Physiol.* 268:C1313–C1319.

21. Pruvot, E. J., R. P. Katra, D. S. Rosenbaum, and K. R. Laurita. 2004. Role of calcium cycling versus restitution in the mechanism of repolarization alternans. *Circ. Res.* 94:1083–1090.

22. Ghosh, S., D. A. Nunziato, and G. S. Pitt. 2006. KCNQ1 assembly and function is blocked by long-QT syndrome mutations that disrupt interaction with calmodulin. *Circ. Res.* 98:1048–1054.

23. Shamgar, L., L. Ma, N. Schmitt, Y. Haitin, A. Peretz, R. Wiener, J. Hirsch, O. Pongs, and B. Attali. 2006. Calmodulin is essential for cardiac I_{Ks} channel gating and assembly: impaired function in long-QT mutations. *Circ. Res.* 98:1055–1063.

24. Shiferaw, Y., D. Sato, and A. Karma. 2005. Coupled dynamics of voltage and calcium in paced cardiac cells. *Phys. Rev. E.* 71:021903.

25. Qu, Z., and J. N. Weiss. 2005. Effects of Na and K channel blockade on vulnerability to and termination of fibrillation in simulated normal cardiac tissue. *Am. J. Physiol.* 289:H1692–H1701.

26. Sato, D., Y. Shiferaw, A. Garfinkel, J. N. Weiss, Z. Qu, and A. Karma. 2006. Spatially discordant alternans in cardiac tissue. Role of calcium cycling. *Circ. Res.* 99:520–527.

27. Splawski, I., K. W. Timothy, N. Decher, P. Kumar, F. B. Sachse, A. H. Beggs, M. C. Sanguinetti, and M. T. Keating. 2005. Severe arrhythmia disorder caused by cardiac L-type calcium channel mutations. *Proc. Natl. Acad. Sci. USA.* 102:8089–8096.